

BlindSight: Harnessing Sparsity for Efficient VLMs

Tharun Adithya Srikrishnan* Deval Shah* Steven K. Reinhardt
Advanced Micro Devices, Inc. (AMD)

Abstract

Large vision-language models (VLMs) enable the joint processing of text and images. However, the inclusion of vision data significantly expands the prompt length. Along with the quadratic complexity of the attention computation, this results in a longer prefill duration. An approach to mitigate this bottleneck is to leverage the inherent sparsity in the attention computation. In our analysis of attention patterns in VLMs, we observe that a substantial portion of layers exhibit minimal cross-image attention, except through attention-sink tokens per image. These sparse attention patterns fall into distinct categories: sink-only, document mask and a hybrid document-sink mask. Based on this, we propose **BlindSight**: a training-free approach to optimize VLM inference using an input-template-aware attention sparsity mask. We utilize samples from a dataset to derive a prompt-agnostic sparsity categorization for every attention head. We evaluate the proposed technique using VLMs such as Qwen2-VL, Qwen2.5-VL and Gemma-3. BlindSight results in a 32 – 41% reduction in FLOPs on average with $\pm 2\%$ accuracy compared to the original model in most evaluated multi-image understanding benchmarks.

1 Introduction

Vision-language models (VLMs) have shown impressive capabilities in processing visual and textual information together [1, 2, 3, 4, 5]. This has opened up several avenues for application in fields such as autonomous driving [6, 7], finance [8, 9], medical research [10, 11] and robotics [12, 13]. VLMs often incorporate pre-trained vision encoders, with a transformer-based multimodal processing module to process both language and vision tokens. The context lengths in VLMs are expected to be significantly higher due to the large number of tokens introduced by images. Practical applications utilizing videos or high-resolution images will further increase the context length.

Attention dominates during inference for longer context lengths due to its quadratic computational complexity. The time-to-first-token (TTFT) (i.e., prefill time) for such prompts can be in the order of minutes and may even require distributed attention computation [14, 15]. In Llama2-7B [16], the attention operation accounts for 70% of the total prefill time when processing an input of 64K tokens. The real-time application of VLMs is therefore limited due to the increased TTFT. An additional consequence of the increased context length is the substantial increase in the KV cache size during the decode phase, which further increases the system memory requirements. This impact is expected to only worsen with the test-time scaling paradigm [17, 18, 19, 20]. In this study, our focus lies on optimizing the prefill phase of VLM inference for text with multi-image input scenarios.

VLMs differ from LLMs in that their inputs typically consist of a sequence of interleaved images and text. The length of each image segment may vary depending on the image resolution and tokenization approach. Prior works have observed that attention matrices tend to be sparse [21, 22]. We observe this phenomenon in VLMs as well, as shown in Figure 1a. This sparsity can be exploited to accelerate the prefill time by masking out computations corresponding to the sparse

*Equal contribution

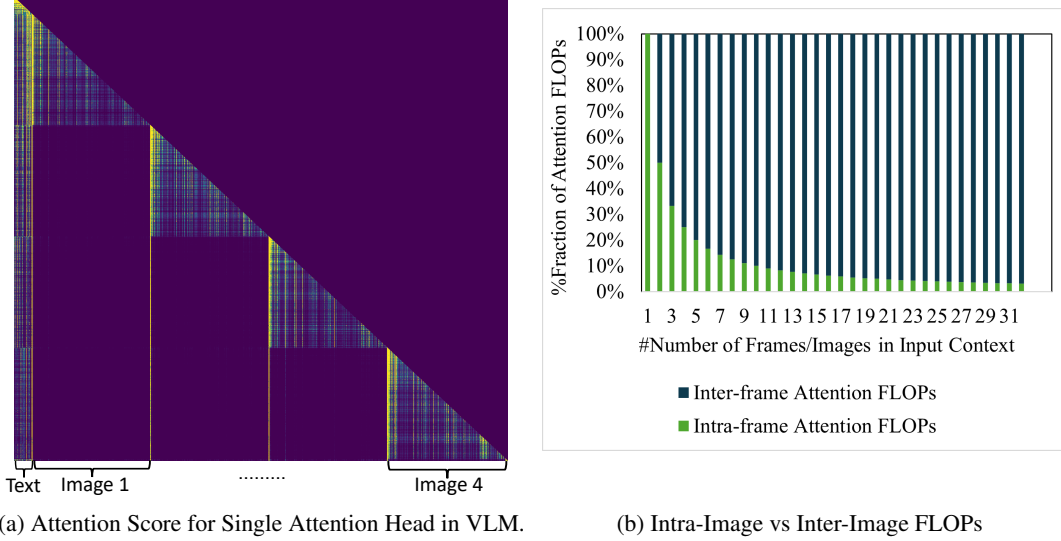


Figure 1: (a) Attention score for an attention head in Qwen2.5-VL (7B). The input prompt consists of text followed by 4 images. Notice that the image tokens vastly outnumber text tokens. (b) The impact of number of inputs images on intra- and inter-image attention floating point operations (FLOPs) , for longer context, inter-image attention contributed to more than 97% of the attention FLOPs.

elements. Existing VLM-specific sparsity-based optimization techniques such as MMInference [23] and Look-M [24] rely on computing partial attention score-based metrics during inference to identify intra-modality sparsification opportunities at the cost of additional computation.

We observe that inter-image attention dominates the overall attention computation as the number of images in the prompt increases (Figure 1b). Based on this observation, we specifically focus on inter-image sparsity patterns in the text-vision multimodal transformer. We characterize the attention matrix for several multi-image VLMs such as Qwen2-VL [1], Qwen2.5-VL [2] and Gemma 3 [4]. We then categorize these sparsity patterns to derive distinct groups defined by the input prompt template (i.e., from the position of the text and images). We find that these patterns can be classified using a combination of intra-image and inter-image patterns: a diffuse pattern or a sparse *Sink*, *Document* or *Document-Sink* pattern (Section 3). We also observe an input-dependent variation in the optimal sparsity template selected per head. We observe that a carefully designed aggregation scheme can transform the prompt-dependent mask-template choice into a prompt-independent one (Section 4):

- **Prompt-level Characterization:** Metric-based approach to select the most computationally efficient sparsity mask per head with minimum accuracy impact.
- **Dataset-level Aggregation:** Rule-based approach to aggregate prompt-level mask categorizations across a mask-characterization dataset.

We demonstrate the efficacy of BlindSight on multi-image comprehension benchmarks in Section 5. Our contributions can be summarized as follows:

- Characterized inter-image attention patterns for several VLMs and identified four attention mask categories: *Dense*, *Sink*, *Document* and *Document-Sink*. The proposed masks can be constructed from input prompt tokens without additional inference-time computation.
- Developed **BlindSight**, an approach to select the optimal attention mask-type per attention head in VLMs using an offline characterization flow. Our approach results in negligible accuracy impacts despite prompt-level sparsity variations.
- Investigated the underlying sources of this sparsity, emphasizing the role of modality boundary tokens, which function as attention sinks per image.

2 Related Work

Static Attention Sparsity in LLMs: Static sparsity-based post-training model optimizations rely on offline characterization to identify fixed sparsity patterns to be used during inference. The sliding window attention layer introduced in LongFormers [22] computed the attention using only the most recent keys per query. Sparse Transformer [25] employs a strided pattern along with windowing for efficient computation. Big Bird [21] enhances the sliding window approach by incorporating random blocks to capture block sparsity. Streaming LLM [26] highlighted the role of sink tokens, early tokens that garner high attention scores [27]. This insight can be used to confine computation to an A-shaped segment of the overall attention. While static sparsity patterns generally result in coherent conversations and efficient computation, they show poor performance on LLM benchmarks.

Dynamic Sparsity in LLMs: Dynamic sparsity techniques rely on additional inference-time metrics to derive an input-dependent attention sparsity mask. DuoAttention [28] seeks to address gaps in static sparsity by classifying attention heads into streaming heads (A-shaped) and retrieval heads (full attention) through fine-tuning. SnapKV [29] proposes compressing the KV cache by selecting clustered KV positions for each head. MInference [30] proposes to categorize each head during inference into three types: A-shaped, block sparse, and vertical-slash; though the vertical-slash pattern proves to be sufficient in practice. Furthermore, attention sparsity is also observed in the KV cache during the decode phase. Techniques such as H2O [31], ScissorHands [32] and PyramidKV [33] prune out past tokens using attention score-based metrics.

Sparsity in VLMs: MMInference [23] dynamically derives intra-modality sparse patterns, similar to MInference, while augmenting them with static cross-modality sparsity patterns. The identification of the static sparsity patterns per head is conducted offline on a single sample. However, online computation is required to identify the intra-modality grid-like sparsity pattern. Look-M [24] optimizes the KV cache for VLMs using a KV cache merging scheme.

3 Attention and Sparsity in VLMs

VLM prompts are composed of interleaved text and images. With a specific focus on inter-image interactions, we visually studied the attention matrix across layers for a variety of inputs. Although precise conclusions on sparsity masks can only be derived by studying the attention output, the attention matrix provides a visual proxy for analysis. Fig. 2 represents examples of the attention matrix for different types of sparse heads in Qwen2-VL [1]. We observe that these patterns remain consistent across other VLMs such as Qwen2.5-VL, and Gemma 3. We observe that attention heads in VLMs belong to two categories, **Diffuse heads** and **Sparse heads**:

- **Diffuse heads** have no discernible pattern of low-valued elements in the attention matrix, or consist of patterns that are not repeated across models and layers
- **Sparse heads** have many low-valued elements, and exhibit distinct boundaries at the text-image and image-image interface. They can be broadly categorized into three groups: **Sink heads**, **Document Mask heads** and **Document-Sink heads**.

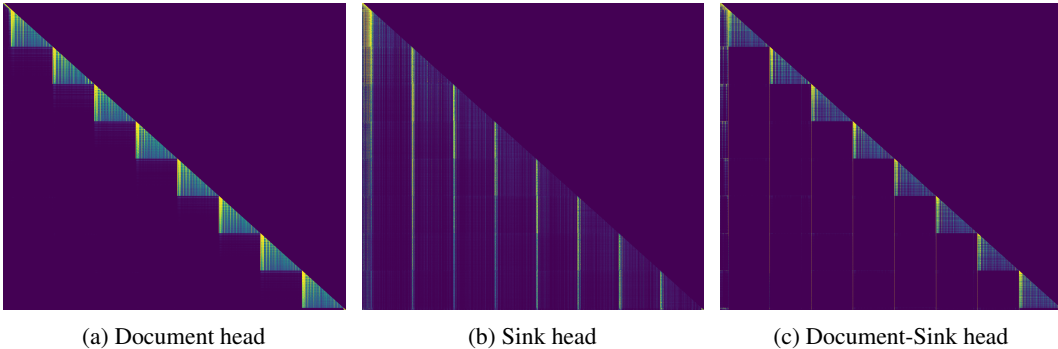


Figure 2: Sparse attention head categories in VLMs for text with multi-image inputs.

We further observe that variations exist in the sparsity patterns for sparse heads with different inputs. However, a single category tends to dominate every head for a given model. Further analysis of **Sparse heads** reveals that text-to-image or image-to-image transitions are frequently followed by an attention sink [26]. We discuss this aspect in Section 6. We do not observe any notable image-to-image attention beyond these attention sinks. **Sink heads** exhibit only this attention-sink behavior, with no intra-image attention. These heads possibly specialize in pooling information. **Document heads** only attend within each image, with no sink based cross-image attention. These types of heads are similar to masks used during sequence packing during LLM training. These heads focus mostly on intra-image processing. **Document-Sink heads** combine both the attention sink and document patterns per image. These heads both focus on processing data and pooling information. These sparsity categories offer a template for creating a mask based on the positions of the text and image tokens in the prompt. Note that the model’s original masking approach (dense attention) can be used to handle diffuse heads.

We can take advantage of the rich sparsity available in VLMs by masking out computations in sparse attention heads that contribute negligibly to the final attention score. BlindSight optimizes cross-image attentions, and its impact is particularly evident in multi-image scenarios dominated by cross-image attention (Figure 1b). The impact of optimizing intra-image attentions using grid-like sparsity patterns [23] appears relatively modest for longer contexts dominated by images.

4 BlindSight

With insights from Section 3, we propose BlindSight. The approach consists of two steps: prompt-level characterization and dataset-level aggregation. The first step involves characterizing attention heads for a single prompt. We aim to identify the optimal sparsity mask from the four categories. Given variations in the mapping for different prompts, we then derive a single attention head to mask-type mapping across a characterization dataset by aggregating individual prompt-level categorizations.

4.1 Prompt-level Characterization

Although visual characterization can provide valuable insights, practical deployments require an algorithmic approach to determine the optimal attention sparsity pattern. BlindSight addresses this need by minimizing the difference between the baseline dense attention output and the proposed sparse attention. Aligning outputs at each layer intuitively ensures that the overall model output remains aligned. Additionally, the algorithm prioritizes the sparsity mask that achieves the lowest theoretical total floating point operations (FLOPs), provided that it achieves a specified minimum performance. A threshold α on the normalized mean squared error (NMSE) serves as the selection criterion. We return to the original dense mask, corresponding to diffuse attentions, when no sparse mask achieves an NMSE below α . Algorithm 1 describes the approach to identify the mask-type for every attention head in a model, given a prompt with sequence length S and a model with a hidden dimension d_h .

Algorithm 1 BlindSight: Prompt-level Characterization

Input: layer; head; $Q, K, V \in \mathcal{R}^{S \times d_h}$
Output: Mask_type[layer][head]
 $A_{\text{ref}} = \text{SoftMax}(\text{DenseMask}(QK^T)V)$
mask_type[layer][head] = 'Dense'
for mask \in ['Sink', 'Document', 'Document-Sink'] **do**
 $A_{\text{mask}} = \text{SoftMax}(\text{mask}(QK^T)V)$
 $\text{NMSE}_{\text{mask}} = \frac{\|A_{\text{mask}} - A_{\text{ref}}\|_2^2}{\|A_{\text{ref}}\|_2^2}$
if $\text{NMSE}_{\text{mask}} < \alpha$ **then**
mask_type[layer][head] = mask
break
end if
end for
return mask_type[layer][head]

4.2 Dataset-level Aggregation

We repeat the prompt-level characterization on a dataset to investigate the variation in masks selected for different prompts. For this characterization, we use samples from the Multimodal Multi-image Understanding (MMIU) benchmark [34], which is designed to evaluate multi-image comprehension. Fig. 3 represents the distribution of the mask type selected for different attention heads across the entire data set. Most layers exhibit a preference for a single dominant mask type across samples. In certain layers, however, we observe that the dense mask is preferred for a non-negligible fraction, even though it is not the predominant choice.

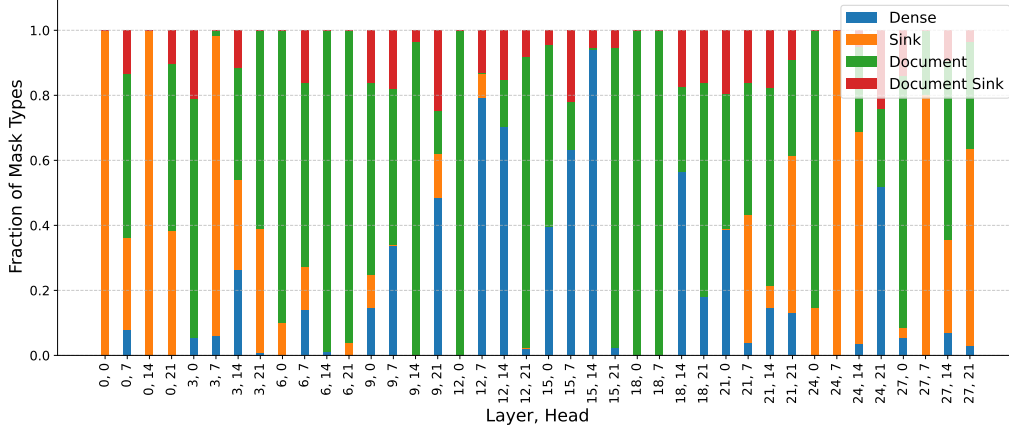


Figure 3: Distribution of sparse mask categories shown for select attention heads across the MMIU dataset using the prompt-level characterization scheme.

We propose an intuitive rule-based aggregation algorithm based on the distribution of masks selected across prompts. For every layer, we rely on the predominant attention mask selected across the dataset, with the exception of instances where the dense mask exceeds a specified threshold fraction. This cautious strategy mitigates potential performance degradations associated with excessive sparsification. In scenarios where neither the sink nor the document mask dominates, we revert to the superset document-sink category.

Algorithm 2 BlindSight: Dataset-level Aggregation

```

Input: layer; head; mask_fraction
if mask_fraction[layer][head]['Dense'] >  $\gamma_c$  then
    return 'Dense'
end if
if mask_fraction[layer][head]['Sink'] >  $\gamma_s$  then
    return 'Sink'
end if
if mask_fraction[layer][head]['Document'] >  $\gamma_d$  then
    return 'Document'
else
    return 'Document-Sink'
end if

```

Based on this aggregation, we observe that 60% of every model consists of sparse heads (Figure 4). This characterization was derived using the configurations discussed in Section 5. Algorithm parameters (α , γ_c , γ_s , γ_d) can be used to trade off sparsity and accuracy. Note that the mapping is derived using a single characterization dataset and is held fixed while evaluating benchmarks.

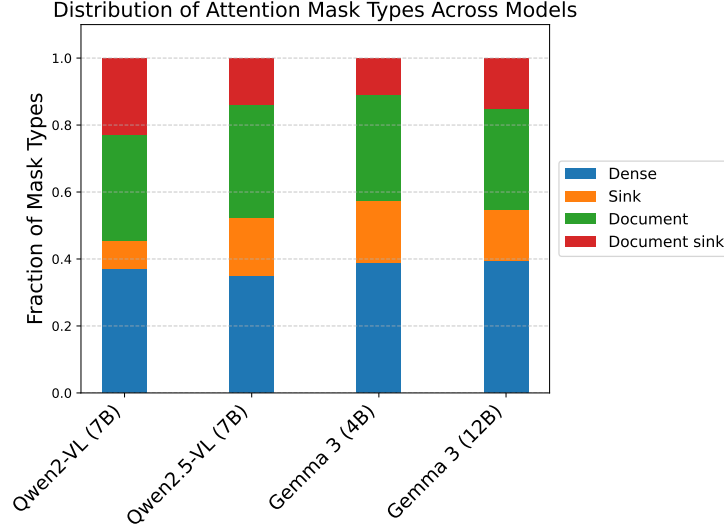


Figure 4: Distribution of Sparsity Categories Across VLMs.

5 Performance Evaluation

5.1 Experimental Setup

Models We use open-source models available through Hugging Face [35] to implement our proposed solution. The experiments focus on Qwen2-VL (7B) [1], Qwen2.5-VL (7B) [2], and Gemma 3 (4B, 12B) [4]. All of these models employ transformer-based joint processing of vision embeddings (derived from a vision encoder) and text embeddings.

Implementation We utilize attention mechanisms specific to each model within the Hugging Face Transformers library [35] to develop a custom attention mask variant. This custom sparse attention layer is integrated into the base model via monkey-patching. The current approach is based on native PyTorch [36]. While this enabled rapid iteration, the materialization of attention matrices limits the maximum sequence length due to memory constraints. We aim to replace this with an optimized kernel in the near future.

Sparsity Mask Generation The proposed sparse attention mask template requires knowing the positions of text and images within the prompt. These positions are determined by identifying the `<image_start>` and `<image_end>` tokens within the tokenized prompt. Each type of sparse mask (sink, document, document-sink) employs a different implementation based on these positions. The specific sparse mask per head is available through the attention characterization described previously. The attention sink for every image is set to 10% of the corresponding image length. Note that we currently only aim to optimize prefill time for VLMs and retain the entire KV cache.

The position of attention sinks in sparse layers depends upon the specific implementation and training recipe used in the model. For the Qwen family of models, the attention sinks always occur at the start of the image. Unlike other VLMs, Gemma 3 tokenizes every image to the same length and employs a non-causal full attention mechanism within an image. The attention sinks here occur at fixed locations within every image as shown in Fig. 7. We characterized the location of attention sinks using the MMIU [34] dataset, and selected the top 10% of the highest frequency sink positions.

Infrastructure The experiments were carried out on an AMD Instinct MI300X node with 8 GPUs. We utilized a PyTorch container with ROCm installed for development and experimentation. With 192 GB of HBM, we were able to load the entire model onto a single GPU for visual analysis. For visual understanding benchmarks discussed below, we use the Hugging Face model sharder to distribute the model across the GPUs.

Hyper-parameter Selection Hyper-parameters allow for trading off accuracy and sparsity. Prompt level characterization requires setting the NMSE selection threshold α . We empirically set the selection threshold to 10%, that is, α of 0.1. In the dataset level aggregation step, we set γ_c to 0.25; γ_s and γ_d to 0.60.

5.2 Benchmarks

BlindSight is a prefill optimization strategy that specifically impacts scenarios involving image-to-image interactions. We therefore evaluate BlindSight using a variety of multi-image understanding benchmarks. These benchmarks typically present a sequence of images accompanied by a multiple-choice question pertaining to the image content. Specifically, the MMIU [34], MUIRBench [37], BLINK [38], and MANTIS-eval [39] benchmarks are used to assess VLM comprehension across diverse categories and prompt lengths. For now, we limit our benchmarks to samples under 5000 tokens due to the memory requirements of the native PyTorch-based eager attention implementation. The results shown in Table 1 highlight the performance of BlindSight on these benchmarks.

Table 1: Accuracy (%) on Multi-Image Comprehension Benchmarks.

Qwen2-VL (7B)				
	MMIU	MANTIS	MUIRBench	BLINK
Original	37.40	67.77	46.24	36.12
BlindSight	35.51	65.40	45.73	37.48

Qwen2.5-VL (7B)				
	MMIU	MANTIS	MUIRBench	BLINK
Baseline	35.39	72.51	54.77	39.20
BlindSight	36.14	72.99	53.39	38.20

Gemma 3 (4B)				
	MMIU	MANTIS	MUIRBench	BLINK
Original	35.40	63.98	41.05	35.08
BlindSight	34.56	59.00	39.24	30.57

Gemma 3 (12B)				
	MMIU	MANTIS	MUIRBench	BLINK
Original	36.07	69.67	50.32	51.83
BlindSight	34.73	68.25	48.14	47.28

In the case of Qwen-type models, accuracy degradations are limited to 2%, suggesting that a large portion of the masked-out computations have minimal impact on the final prediction. Select benchmarks even show improvements, likely due to the regularization enforced by the sparse masks. In the case of the Gemma models, the BLINK benchmark suffers significantly with sparsification.

5.3 Theoretical FLOPs Reduction

The potential practical performance improvements gained from BlindSight can be demonstrated by examining the savings in theoretical FLOPs. The theoretical FLOPs reduction for each head is calculated by determining the proportion of the attention computation that is masked out. The extent of masking for a given prompt depends on the number of images, the tokens per image, and the length of the interleaved text. The algorithm is detailed in Appendix A. It is important to note that each attention head may exhibit a unique sparsity pattern at the model level.

We estimate model-level savings using BlindSight by combining the FLOPs reduction for each mask type, weighted by their respective occurrence within the model. That is, $\text{Total_FLOPs_reduction} = \sum_{\text{mask}} \text{fraction}[\text{mask}] \cdot \text{FLOPs_reduction}[\text{mask}]$. The cumulative distribution function (CDF) of the FLOPs reduced for Qwen2.5-VL computed on the MMIU dataset [34] is shown in Figure 5. Our analysis reveals comparable mean savings in FLOPs across VLMs: Qwen2-VL-7B (32%), Qwen2.5-VL-7B (35%), Gemma 3-4B (39%) and Gemma 3-12B (41%).

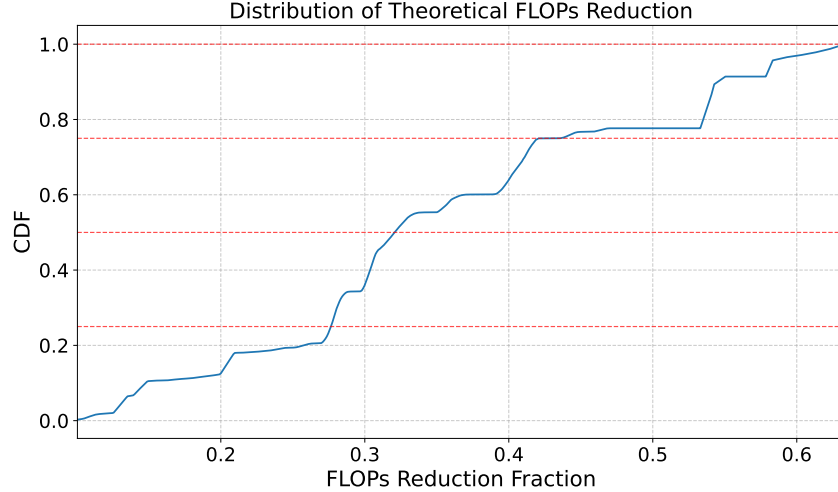


Figure 5: Theoretical FLOPs Reduction Using BlindSight on the MMIU Dataset for Qwen2.5-VL.

6 Discussion

Attention sinks emerge in large models during pre-training, where the SoftMax operator is repeatedly applied on the early tokens [26]. Additionally, massive activations occur independent of input data within specific attention layers. These activations develop into sinks that function as implicit bias terms within the attention layer [40]. Furthermore, delimiter tokens (punctuation, `\n`) with low semantic value often correspond to high attention scores [41]. Recent evidence [42, 43] highlights the crucial role of the attention sink in long-context learning.

We now empirically study the role of attention sinks associated with every image. VLM prompts typically consist of delimiter tokens at the start (`<image_start>`) and end (`<image_end>`) of every image. We hypothesize that the image boundary tokens are essential for enabling sparsity. In order to support this claim, we remove these boundary tokens in a text-image interleaved prompt in Qwen2-VL (7B). We observe that document masking, i.e the intra-image attention, ceases to exist. Partial information pooling across images still persists via weak sinks. We observe a significant degradation of the Document and Document-Sink patterns, resulting in partial or incoherent responses.

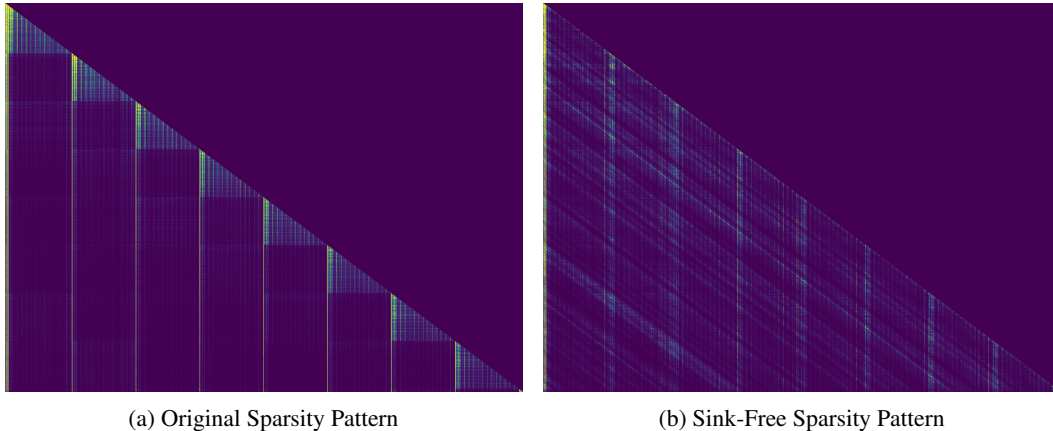


Figure 6: Impact of Removing Image Boundary Tokens: Removing `<image_start>` and `<image_end>` impairs attention sinks and disrupts the document-masking pattern.

BlindSight offers significant performance enhancements by sparsifying a VLM post-training. However, we advocate for incorporating sparsity directly into the model architecture. Llama 4 [3] includes chunked attention (document masking) layers, which also enable linear scaling in complexity at long sequence lengths. Native Sparse Attention [44] directly incorporates static and dynamic sparsity into

the attention mechanism. Models can be composed through a mixture of low-complexity attention layers and dense attention layers, as evidenced in Figure 4. Post-training sparsification [28] and hybrid state-space based models [45, 46, 47] highlight the potential to achieve improved efficiency and performance by strategically combining sparse and dense attention mechanisms.

7 Conclusion

We investigated inter-image interactions within the attention layers of VLMs. From this analysis, we developed BlindSight: an input-template-based VLM sparsification technique that achieves performance levels comparable to dense attention across various multi-image understanding benchmarks. We are currently expanding this work to evaluate performance on long-context multimodal benchmarks and developing efficient implementations.

References

- [1] Peng Wang, Shuai Bai, Sinan Tan, Shijie Wang, Zhihao Fan, Jinze Bai, Keqin Chen, Xuejing Liu, Jialin Wang, Wenbin Ge, Yang Fan, Kai Dang, Mengfei Du, Xuancheng Ren, Rui Men, Dayiheng Liu, Chang Zhou, Jingren Zhou, and Junyang Lin. Qwen2-VL: Enhancing Vision-Language Model’s Perception of the World at Any Resolution, 2024.
- [2] Shuai Bai, Keqin Chen, Xuejing Liu, Jialin Wang, Wenbin Ge, Sibao Song, Kai Dang, Peng Wang, Shijie Wang, Jun Tang, Humen Zhong, Yuanzhi Zhu, Mingkun Yang, Zhaohai Li, Jianqiang Wan, Pengfei Wang, Wei Ding, Zheren Fu, Yiheng Xu, Jiabo Ye, Xi Zhang, Tianbao Xie, Zesen Cheng, Hang Zhang, Zhibo Yang, Haiyang Xu, and Junyang Lin. Qwen2.5-VL Technical Report, 2025.
- [3] Meta AI. Llama 4 Models: Model Card and Documentation. https://github.com/meta-llama/llama-models/blob/main/models/llama4/MODEL_CARD.md, 2025. Accessed: 2025-06-24.
- [4] Gemma Team. Gemma 3 Technical Report, 2025.
- [5] Zhe Chen, Jiannan Wu, Wenhai Wang, Weijie Su, Guo Chen, Sen Xing, Muyan Zhong, Qinglong Zhang, Xizhou Zhu, Lewei Lu, Bin Li, Ping Luo, Tong Lu, Yu Qiao, and Jifeng Dai. InternVL: Scaling up Vision Foundation Models and Aligning for Generic Visual-Linguistic Tasks, 2024.
- [6] Anthony Hu, Lloyd Russell, Hudson Yeo, Zak Murez, George Fedoseev, Alex Kendall, Jamie Shotton, and Gianluca Corrado. GAIA-1: A Generative World Model for Autonomous Driving, 2023.
- [7] Xiaoyu Tian, Junru Gu, Bailin Li, Yicheng Liu, Yang Wang, Zhiyong Zhao, Kun Zhan, Peng Jia, Xianpeng Lang, and Hang Zhao. DriveVLM: The Convergence of Autonomous Driving and Large Vision-Language Models, 2024.
- [8] Ziao Wang, Yuhang Li, Junda Wu, Jaehyeon Soon, and Xiaofeng Zhang. FinVis-GPT: A Multimodal Large Language Model for Financial Chart Analysis, 2023.
- [9] Gagan Bhatia, El Moatez Billah Nagoudi, Hasan Cavusoglu, and Muhammad Abdul-Mageed. FinTral: A Family of GPT-4 Level Multimodal Financial Large Language Models, 2024.
- [10] Jean-benoit Delbrouck, Khaled Saab, Maya Varma, Sabri Eyuboglu, Pierre Chambon, Jared Dunnmon, Juan Zambrano, Akshay Chaudhari, and Curtis Langlotz. ViLMedic: a framework for research at the intersection of vision and language in medical AI. In *Proceedings of the 60th Annual Meeting of the Association for Computational Linguistics: System Demonstrations*, pages 23–34, Dublin, Ireland, May 2022. Association for Computational Linguistics.
- [11] Iryna Hartsock and Ghulam Rasool. Vision-language models for medical report generation and visual question answering: a review. *Frontiers in Artificial Intelligence*, 7, November 2024.

- [12] Kevin Black, Noah Brown, Danny Driess, Adnan Esmail, Michael Equi, Chelsea Finn, Niccolo Fusai, Lachy Groom, Karol Hausman, Brian Ichter, Szymon Jakubczak, Tim Jones, Liyiming Ke, Sergey Levine, Adrian Li-Bell, Mohith Mothukuri, Suraj Nair, Karl Pertsch, Lucy Xiaoyang Shi, James Tanner, Quan Vuong, Anna Walling, Haohuan Wang, and Ury Zhilinsky. π_0 : A Vision-Language-Action Flow Model for General Robot Control, 2024.
- [13] Anthony Brohan, Noah Brown, Justice Carbajal, Yevgen Chebotar, Xi Chen, Krzysztof Choromanski, Tianli Ding, Danny Driess, Avinava Dubey, Chelsea Finn, Pete Florence, Chuyuan Fu, Montse Gonzalez Arenas, Keerthana Gopalakrishnan, Kehang Han, Karol Hausman, Alexander Herzog, Jasmine Hsu, Brian Ichter, Alex Irpan, Nikhil Joshi, Ryan Julian, Dmitry Kalashnikov, Yuheng Kuang, Isabel Leal, Lisa Lee, Tsang-Wei Edward Lee, Sergey Levine, Yao Lu, Henryk Michalewski, Igor Mordatch, Karl Pertsch, Kanishka Rao, Krista Reymann, Michael Ryoo, Grecia Salazar, Pannag Sanketi, Pierre Sermanet, Jaspiar Singh, Anikait Singh, Radu Soricut, Huong Tran, Vincent Vanhoucke, Quan Vuong, Ayzaan Wahid, Stefan Welker, Paul Wohlhart, Jialin Wu, Fei Xia, Ted Xiao, Peng Xu, Sichun Xu, Tianhe Yu, and Brianna Zitkovich. RT-2: Vision-Language-Action Models Transfer Web Knowledge to Robotic Control, 2023.
- [14] Hao Liu, Matei Zaharia, and Pieter Abbeel. RingAttention with Blockwise Transformers for Near-Infinite Context. In *The Twelfth International Conference on Learning Representations*, 2024.
- [15] William Brandon, Aniruddha Nrusimha, Kevin Qian, Zachary Ankner, Tian Jin, Zhiye Song, and Jonathan Ragan-Kelley. Striped Attention: Faster Ring Attention for Causal Transformers, 2023.
- [16] Meta AI. Llama 2: Open Foundation and Fine-Tuned Chat Models, 2023.
- [17] Charlie Snell, Jaehoon Lee, Kelvin Xu, and Aviral Kumar. Scaling LLM Test-Time Compute Optimally can be More Effective than Scaling Model Parameters, 2024.
- [18] Shunyu Yao, Dian Yu, Jeffrey Zhao, Izhak Shafran, Thomas L. Griffiths, Yuan Cao, and Karthik Narasimhan. Tree of Thoughts: Deliberate Problem Solving with Large Language Models, 2023.
- [19] Niklas Muennighoff, Zitong Yang, Weijia Shi, Xiang Lisa Li, Li Fei-Fei, Hannaneh Hajishirzi, Luke Zettlemoyer, Percy Liang, Emmanuel Candès, and Tatsunori Hashimoto. s1: Simple test-time scaling, 2025.
- [20] Ranajoy Sadhukhan, Zhuoming Chen, Haizhong Zheng, Yang Zhou, Emma Strubell, and Beidi Chen. Kinetics: Rethinking Test-Time Scaling Laws, 2025.
- [21] Manzil Zaheer, Guru Guruganesh, Avinava Dubey, Joshua Ainslie, Chris Alberti, Santiago Ontanon, Philip Pham, Anirudh Ravula, Qifan Wang, Li Yang, and Amr Ahmed. Big Bird: Transformers for Longer Sequences, 2021.
- [22] Iz Beltagy, Matthew E. Peters, and Arman Cohan. Longformer: The Long-Document Transformer, 2020.
- [23] Yucheng Li, Huiqiang Jiang, Chengruidong Zhang, Qianhui Wu, Xufang Luo, Surin Ahn, Amir H. Abdi, Dongsheng Li, Jianfeng Gao, Yuqing Yang, and Lili Qiu. MMInference: Accelerating Pre-filling for Long-Context VLMs via Modality-Aware Permutation Sparse Attention, 2025.
- [24] Zhongwei Wan, Ziang Wu, Che Liu, Jinfa Huang, Zhihong Zhu, Peng Jin, Longyue Wang, and Li Yuan. LOOK-M: Look-Once Optimization in KV Cache for Efficient Multimodal Long-Context Inference, 2024.
- [25] Rewon Child, Scott Gray, Alec Radford, and Ilya Sutskever. Generating Long Sequences with Sparse Transformers, 2019.
- [26] Guangxuan Xiao, Yuandong Tian, Beidi Chen, Song Han, and Mike Lewis. Efficient Streaming Language Models with Attention Sinks, 2024.

- [27] Jesse Vig and Yonatan Belinkov. Analyzing the Structure of Attention in a Transformer Language Model, 2019.
- [28] Guangxuan Xiao, Jiaming Tang, Jingwei Zuo, Junxian Guo, Shang Yang, Haotian Tang, Yao Fu, and Song Han. DuoAttention: Efficient Long-Context LLM Inference with Retrieval and Streaming Heads, 2024.
- [29] Yuhong Li, Yingbing Huang, Bowen Yang, Bharat Venkitesh, Acyr Locatelli, Hanchen Ye, Tianle Cai, Patrick Lewis, and Deming Chen. SnapKV: LLM Knows What You are Looking for Before Generation, 2024.
- [30] Huiqiang Jiang, Yucheng Li, Chengruidong Zhang, Qianhui Wu, Xufang Luo, Surin Ahn, Zhenhua Han, Amir H. Abdi, Dongsheng Li, Chin-Yew Lin, Yuqing Yang, and Lili Qiu. MInference 1.0: Accelerating Pre-filling for Long-Context LLMs via Dynamic Sparse Attention, 2024.
- [31] Zhenyu Zhang, Ying Sheng, Tianyi Zhou, Tianlong Chen, Lianmin Zheng, Ruisi Cai, Zhao Song, Yuandong Tian, Christopher Ré, Clark Barrett, Zhangyang Wang, and Beidi Chen. H₂O: Heavy-Hitter Oracle for Efficient Generative Inference of Large Language Models, 2023.
- [32] Zichang Liu, Aditya Desai, Fangshuo Liao, Weitao Wang, Victor Xie, Zhaozhuo Xu, Anastasios Kyrillidis, and Anshumali Shrivastava. Scissorhands: Exploiting the Persistence of Importance Hypothesis for LLM KV Cache Compression at Test Time, 2023.
- [33] Zefan Cai, Yichi Zhang, Bofei Gao, Yuliang Liu, Yucheng Li, Tianyu Liu, Keming Lu, Wayne Xiong, Yue Dong, Junjie Hu, and Wen Xiao. PyramidKV: Dynamic KV Cache Compression based on Pyramidal Information Funneling, 2025.
- [34] Fanqing Meng, Jin Wang, Chuanhao Li, Quanfeng Lu, Hao Tian, Jiaqi Liao, Xizhou Zhu, Jifeng Dai, Yu Qiao, Ping Luo, Kaipeng Zhang, and Wenqi Shao. MMIU: Multimodal Multi-image Understanding for Evaluating Large Vision-Language Models, 2024.
- [35] Thomas Wolf, Lysandre Debut, Victor Sanh, Julien Chaumond, Clement Delangue, Anthony Moi, Pierric Cistac, Tim Rault, Rémi Louf, Morgan Funtowicz, Joe Davison, Sam Shleifer, Patrick von Platen, Clara Ma, Yacine Jernite, Julien Plu, Canwen Xu, Teven Le Scao, Sylvain Gugger, Mariama Drame, Quentin Lhoest, and Alexander M. Rush. HuggingFace’s Transformers: State-of-the-art Natural Language Processing, 2020.
- [36] Adam Paszke, Sam Gross, Francisco Massa, Adam Lerer, James Bradbury, Gregory Chanan, Trevor Killeen, Zeming Lin, Natalia Gimelshein, Luca Antiga, Alban Desmaison, Andreas Köpf, Edward Yang, Zach DeVito, Martin Raison, Alykhan Tejani, Sasank Chilamkurthy, Benoit Steiner, Lu Fang, Junjie Bai, and Soumith Chintala. PyTorch: An Imperative Style, High-Performance Deep Learning Library, 2019.
- [37] Fei Wang, Xingyu Fu, James Y. Huang, Zekun Li, Qin Liu, Xiaogeng Liu, Mingyu Derek Ma, Nan Xu, Wenxuan Zhou, Kai Zhang, Tianyi Lorena Yan, Wenjie Jacky Mo, Hsiang-Hui Liu, Pan Lu, Chunyuan Li, Chaowei Xiao, Kai-Wei Chang, Dan Roth, Sheng Zhang, Hoifung Poon, and Muhao Chen. MuirBench: A Comprehensive Benchmark for Robust Multi-image Understanding, 2024.
- [38] Xingyu Fu, Yushi Hu, Bangzheng Li, Yu Feng, Haoyu Wang, Xudong Lin, Dan Roth, Noah A. Smith, Wei-Chiu Ma, and Ranjay Krishna. BLINK: Multimodal Large Language Models Can See but Not Perceive, 2024.
- [39] Dongfu Jiang, Xuan He, Huaye Zeng, Cong Wei, Max Ku, Qian Liu, and Wenhui Chen. MANTIS: Interleaved Multi-Image Instruction Tuning, 2024.
- [40] Mingjie Sun, Xinlei Chen, J. Zico Kolter, and Zhuang Liu. Massive Activations in Large Language Models. *arXiv preprint arXiv:2402.17762*, 2024.
- [41] Kevin Clark, Urvashi Khandelwal, Omer Levy, and Christopher D. Manning. What Does BERT Look At? An Analysis of BERT’s Attention, 2019.

- [42] Xiangming Gu, Tianyu Pang, Chao Du, Qian Liu, Fengzhuo Zhang, Cunxiao Du, Ye Wang, and Min Lin. When Attention Sink Emerges in Language Models: An Empirical View, 2025.
- [43] Federico Barbero, Álvaro Arroyo, Xiangming Gu, Christos Perivolaropoulos, Michael Bronstein, Petar Veličković, and Razvan Pascanu. Why do LLMs attend to the first token?, 2025.
- [44] Jingyang Yuan, Huazuo Gao, Damai Dai, Junyu Luo, Liang Zhao, Zhengyan Zhang, Zhenda Xie, Y. X. Wei, Lean Wang, Zhiping Xiao, Yuqing Wang, Chong Ruan, Ming Zhang, Wenfeng Liang, and Wangding Zeng. Native Sparse Attention: Hardware-Aligned and Natively Trainable Sparse Attention, 2025.
- [45] Paolo Glorioso, Quentin Anthony, Yury Tokpanov, James Whittington, Jonathan Pilault, Adam Ibrahim, and Beren Millidge. Zamba: A Compact 7B SSM Hybrid Model, 2024.
- [46] Liliang Ren, Yang Liu, Yadong Lu, Yelong Shen, Chen Liang, and Weizhu Chen. Samba: Simple Hybrid State Space Models for Efficient Unlimited Context Language Modeling, 2025.
- [47] Mingyu Yang, Mehdi Rezagholizadeh, Guihong Li, Vikram Appia, and Emad Barsoum. Zebra-Llama: Towards Extremely Efficient Hybrid Models, 2025.

A Theoretical FLOPs Computation

We highlight the approach followed in computing the savings in FLOPs for models using a causal attention mask as a dense mask for text and images such as Qwen2-VL and Qwen2.5-VL. Similar computations are possible for other models as well.

Algorithm 3 Theoretical FLOPs Reduction for Causal Attention Masks

Input: $\text{img}_{\text{start}}$ (Start positions of images), img_{end} (End positions of images), S
Init.: $\text{masked_area}[\text{'sink'}] = 0$, $\text{masked_area}[\text{'document_sink'}] = 0$, $\text{masked_area}[\text{'document'}] = 0$
Output FLOPs_reduction

```

original_area =  $0.5S^2$ 
for start in range(0, len( $\text{img}_{\text{start}}$ ) - 1) do
    for end in range(start, len( $\text{img}_{\text{end}}$ )) do
        if end = start then
             $\text{masked\_area}[\text{'sink'}] += 0.5 \cdot 0.9 \cdot (\text{img}_{\text{end}}[\text{start}] - \text{img}_{\text{start}}[\text{start}])^2$ 
        else
             $\text{masked\_area}[\text{'document\_sink'}] += 0.9 \cdot (\text{img}_{\text{end}}[\text{start}] - \text{img}_{\text{start}}[\text{start}]) \cdot$ 
                 $(\text{img}_{\text{end}}[\text{end}] - \text{img}_{\text{start}}[\text{end}])$ 
             $\text{masked\_area}[\text{'sink'}] += 0.9 \cdot (\text{img}_{\text{end}}[\text{start}] - \text{img}_{\text{start}}[\text{start}]) \cdot$ 
                 $(\text{img}_{\text{end}}[\text{end}] - \text{img}_{\text{start}}[\text{end}])$ 
        end if
    end for

    for end in range(start + 1, len( $\text{img}_{\text{start}}$ )) do
         $\text{masked\_area}[\text{'document'}] += (\text{img}_{\text{end}}[\text{start}] - \text{img}_{\text{start}}[\text{start}]) \cdot$ 
             $(\text{img}_{\text{end}}[\text{end}] - \text{img}_{\text{start}}[\text{end}])$ 
    end for
end for
 $\text{masked\_area}[\text{'sink'}] += 0.5 \cdot 0.9 \cdot (\text{img}_{\text{end}}[-1] - \text{img}_{\text{start}}[-1])^2$ 
for mask  $\in$  [Sink, Document, Document-Sink] do
    FLOPs_reduction[mask] =  $\text{masked\_area}[\text{mask}] / \text{original\_area}$ 
end for

return FLOPs_reduction

```

B Attention Sink Positions in Gemma 3.

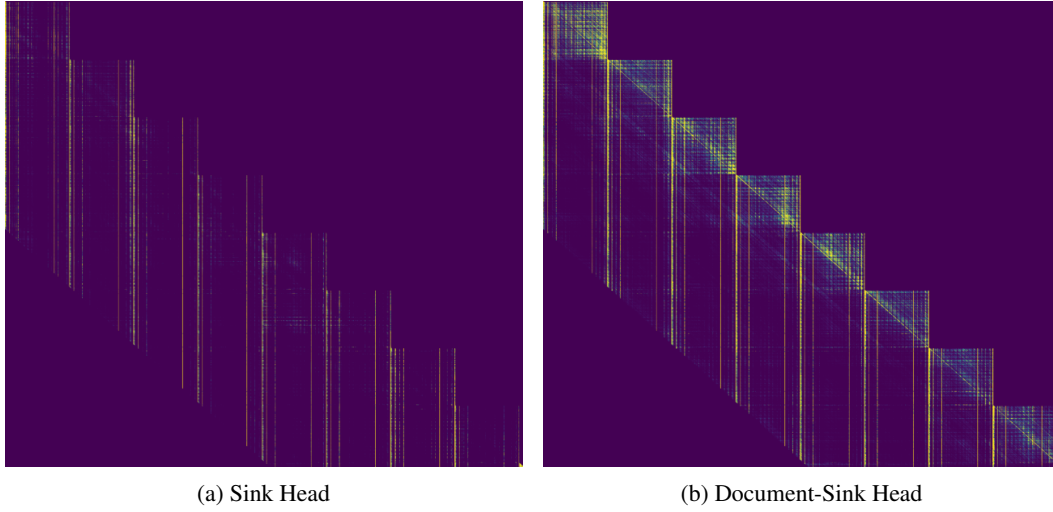


Figure 7: Attention Sink Positions in Gemma 3

Figure 7 represents the attention matrices for different attention heads in the Gemma 3-4B model. As shown in the figure, cross-image attention occurs mainly through attention sinks. However, these attention sinks are located at fixed offsets within the image as opposed to the image boundary in the case of Qwen models.